The Journal of Chemical Physics

Water activation and splitting by single anionic iridium atoms

Cite as: J. Chem. Phys. **157**, 234304 (2022); https://doi.org/10.1063/5.0130277
Submitted: 10 October 2022 • Accepted: 29 November 2022 • Accepted Manuscript Online: 29 November 2022 • Published Online: 16 December 2022

Zhaoguo Zhu (朱兆国), Gaoxiang Liu, Sandra M. Ciborowski, et al.

The Journal of Chemical Physics ARTICLE scitation.org/journal/jcp

Water activation and splitting by single anionic iridium atoms

Cite as: J. Chem. Phys. 157, 234304 (2022); doi: 10.1063/5.0130277
Submitted: 10 October 2022 • Accepted: 29 November 2022 •
Published Online: 16 December 2022

Zhaoguo Zhu (朱兆国), Gaoxiang Liu,[a] Sandra M. Ciborowski,[b] Yulu Cao,[c] Rachel M. Harris, and Kit H. Bowen[d]

AFFILIATIONS

Department of Chemistry, Johns Hopkins University, 3400 N Charles St., Baltimore, Maryland 21218, USA

[a]**Present Address:** Department of Molecular and Cell Biology, Advanced Bioimaging Center, University of California, Berkeley, Barker Hall, Berkeley, CA 94720, USA.
[b]**Present Address:** U.S. Drug Enforcement Agency, Miami, FL 33326, USA.
[c]**Present Address:** Division of Chemistry and Chemical Engineering, California Institute of Technology, Pasadena, CA 91125, USA.
[d]**Author to whom correspondence should be addressed:** kbowen@jhu.edu

ABSTRACT

Mass spectrometric analysis of anionic products that result from interacting Ir^- with H_2O shows the efficient generation of $[Ir(H_2O)]^-$ complexes and IrO^- molecular anions. Anion photoelectron spectra of $[Ir(H_2O)]^-$, formed under various source conditions, exhibit spectral features that are due to three different forms of the complex: the solvated anion–molecule complex, $Ir^-(H_2O)$, as well as the intermediates, $[H–Ir–OH]^-$ and $[H_2–Ir–O]^-$, where one and two O–H bonds have been broken, respectively. The measured and calculated vertical detachment energy values are in good agreement and, thus, support identification of all three types of isomers. The calculated reaction pathway shows that the overall reaction $Ir^- + H_2O \rightarrow IrO^- + H_2$ is exothermic. Two minimum energy crossing points were found, which shuttle intermediates and products between singlet and triplet potential surfaces. This study presents the first example of water activation and splitting by single Ir^- anions.

INTRODUCTION

Water splitting plays a crucial role in the production of hydrogen (H_2), a promising clean and renewable energy source, owing to its carbon-free emission, earth-elemental abundance, and high gravimetric energy density (~142 MJ kg^{-1}). Popular strategies for water splitting include electrolysis,[1–3] photocatalysis,[4,5] artificial photosynthesis,[6,7] and thermal decomposition.[8] However, the industrial application of these methods is impeded by their high energy penalties. To reduce the reaction energy barriers associated with these methods, major efforts have been devoted to developing effective and cost-efficient catalysts.[9–11] In recent years, single-atom catalysts (SACs),[12] especially noble-metal single-atom catalysts (NMSACs),[13] with atomically dispersed metal sites on different substrates, have attracted significant interest, due to their unique physicochemical properties and extremely high atom utilization efficiencies. Among NMSACs, Ir SACs are known to possess extraordinary catalytical performance for water splitting.[14–22] For instance, Ir single atoms, anchored on N-doped, porous carbon supports, dispersed in Co nanoparticles, have displayed an overpotential of 260 mV at 10 mA cm^{-2} for the oxygen evolution reaction (OER), the half-reaction in electrochemical water splitting. This is significantly smaller than that of the commercially used IrO_2 catalyst (385 mV).[15] Additionally, Ir single atoms on $Co_{0.8}Fe_{0.2}Se_2$@Ni foam have been shown to boost the hydrogen evolution reaction (HER)—the critical half-reaction to produce H_2.[16]

The complex conditions that exist in realistic reaction environments prevent detailed insight into the water activation and splitting process. Well-defined, isolated systems in gas phase environments have shown themselves to be useful models for gaining a comprehensive mechanistic understanding of these reactions. Numerous gas-phase studies of water reaction by metal atoms and clusters have provided insights into water splitting at the molecular level.[23–37] Atomic Ni, Pd, and Pt anions have been shown to activate water, leading to water-activated $HMOH^-$ (M = Ni, Pd, and Pt) and H_2MO^- (M = Pt) intermediates. Notably, single Pt anions both

activate and split water, forming H_2 and PtO^- anion products.[38] Inspired by this (our) previous work, we extend the metals to include Ir, providing insight for the designing of more Ir SACs, which may serve as alternatives to Pt SACs. Single neutral and cationic Ir atoms and clusters have been found to react with a variety of small molecules.[39–51] Reactivity of heavy water (D_2O) with single Ir cations measured at room temperature, however, resulted in exclusively simple D_2O solvation adducts, i.e., only $Ir^+(D_2O)$ was observed.[52] Nevertheless, studies on reactions between anionic Ir atoms with water have been unexplored. Herein, we utilize a combination of mass spectroscopy, anion photoelectron spectroscopy, and quantum chemistry calculations, to show that atomic Ir anions both activate and split water.

EXPERIMENTAL METHODS

Experimental studies of $[Ir(H_2O)]^-$ were conducted using an anion photoelectron spectrometer. That apparatus is comprised of several available ion sources, a linear time-of-flight mass spectrometer, a mass gate, a momentum decelerator, a neodymium-doped yttrium aluminum garnet (Nd:YAG) laser for photodetachment, and a magnetic bottle electron energy analyzer having a resolution of 50 meV at EKE = 1 eV.[53] Photoelectron spectra were calibrated against the well-known photoelectron spectrum of Cu^-.[54] The anions in this study were generated using a laser vaporization source, which ablated a rotating, translating iridium metal rod with a pulsed Nd:YAG laser beam operating at a wavelength of 532 nm (2.33 eV). Almost simultaneously, a plume of water vapor-seeded helium gas from a pulsed gas valve (backing pressure of 100 psi) was injected directly over the rod and allowed to flow along a 3 cm tube, where reactions and cooling occurred before products exited into the high vacuum. The resulting anionic clusters were mass-analyzed by the time-of-flight mass spectrometer. After the anions of interest were mass-gated, their photoelectron spectra were measured using the fourth harmonic (4.66 eV photons) of a Nd:YAG laser.

COMPUTATION METHODS

The lowest energy structures of $(Ir–H_2O)^{-/0}$ systems were obtained by density functional theory (DFT)-based electronic structure calculations, with the hybrid functional ωB97x-d.[55,56] The ωB97x-d functional has been tested and has performed well for the IrNOH system.[45] The aug-cc-pvtz basis sets for H and O and the aug-cc-pvtz-pp basis set for Ir were used to optimize all structures.[57–59] All calculations were carried out using the Gaussian 09 software package.[60] The vertical detachment energy (VDE) was obtained by subtracting the electronic energy of the neutral from the anion at its anionic optimized geometry. The electronically excited states of neutral $Ir(H_2O)$ were calculated using the Time-dependent (TD)-DFT method, using the same functional and basis sets. Intrinsic reaction coordinate calculations were employed to check that each transition state (TS) connects two appropriate local minima. Vibrational frequency calculations were performed to check that the intermediates and transition states have zero and only one imaginary frequency, respectively. Natural population analysis (NPA) was conducted to examine the charge distribution at the ωB97x-d level, using natural bond orbital (NBO) 3.1, implemented in Gaussian 09.[61] NPA has been found to be satisfactory in predicting charge distributions within metal-containing clusters.[62,63] The minimum-energy crossing points (MECPs) for the intersection of the electronic states of different spin multiplicities were searched for and located, using the method developed by Harvey *et al.*[64] The electron localization functions (ELF) were analyzed and plotted, employing the Multiwfn program.[65,66]

RESULTS AND DISCUSSION

Experimental

Mass spectra at different iridium rod laser ablation powers are shown in Fig. 1. At low ablation laser power, only Ir^-, $IrOH^-$ and $[Ir(H_2O)]^-$ appear in the mass spectrum. After slightly increasing the laser power, an IrO^- peak also appeared, likely resulting from the decomposition of $[Ir(H_2O)]^-$. The combination of photoelectron spectra and calculations indicated that $[Ir(H_2O)]^-$ in these mass spectra could exist in three forms: (i) an Ir^- anion solvated by a water molecule, i.e., $Ir^-(H_2O)$; (ii) a structure in which only one O–H bond is broken i.e., $[H–Ir–OH]^-$; or (iii) a structure in which two O–H bonds have been broken, i.e., $[H_2–Ir–O]^-$. In the first (i) physisorbed structure, hydrogen atoms in the water molecule only weakly interact with the Ir^- anions. Forms (ii) and (iii) are water-activated products, resulting from one or both O–H bonds being inserted by iridium. All three types of products may possibly co-exist in the ion beam.

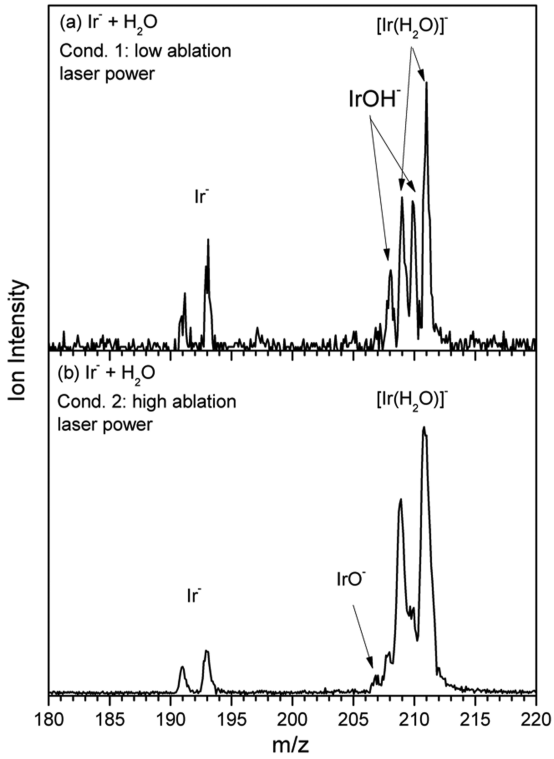

FIG. 1. Mass spectra of an iridium rod being laser ablated in the presence of water vapor. Mass spectrum (a) was recorded under low ablation laser power and (b) under high ablation laser power.

To distinguish between isomers, anion photoelectron spectra were taken under each condition. The middle and bottom panels of Fig. 2 present the anion photoelectron spectra of $[Ir(H_2O)]^-$ at low and high ablation laser power, while the spectrum of the Ir^- atomic anion is displayed in the top panel for comparison. Typically, when an atomic metal anion interacts weakly with another molecule, i.e., when it is physisorbed or solvated, the photoelectron spectral pattern of the resulting anionic complex resembles that of the anion alone, except for being shifted to higher electron binding energy (EBE), with its features slightly broadened. Comparison of the photoelectron spectrum of Ir^- [Fig. 2(a)] and $[Ir(H_2O)]^-$ [Fig. 2(b)] reveal that both spectra exhibit a similar five-peak profile, with all peaks of the $[Ir(H_2O)]^-$ spectrum being broadened and shifted to higher EBE with respect to the Ir^- spectrum. This strong similarity between the two spectra implies that the solvation complex $Ir^-(H_2O)$ is the major product at low laser power conditions (Cond. 1). The maximum intensity of the lowest EBE peak occurs at 2.11 eV; this is designated as the vertical detachment energy (VDE) value of $[Ir–H_2O]^-$. The VDE is the transition energy at which the Franck–Condon overlap is at its maximum between the anion's wave function in its ground electronic state and that of its corresponding neutral at the geometry of the anion, i.e., these are vertical photodetachment transitions. The spectrum in the bottom panel [Fig. 1(c)], on the other hand, has two new peaks, which are denoted as red stars. These two high EBE features at 3.25 and 3.85 eV strongly suggest the presence of activated isomers of $[Ir(H_2O)]^-$, these having been formed at higher laser ablation power conditions (Cond. 2). Therefore, the spectrum displayed in Fig. 2(c) shows features from both physisorbed and chemisorbed products. However, since the full range spectra of activated $[Ir(H_2O)]^-$ species may be buried in the broad physisorbed peaks between 2.0 and 3.0 eV, the VDE values of the activated $[Ir(H_2O)]^-$ species were indeterminate from these spectra.

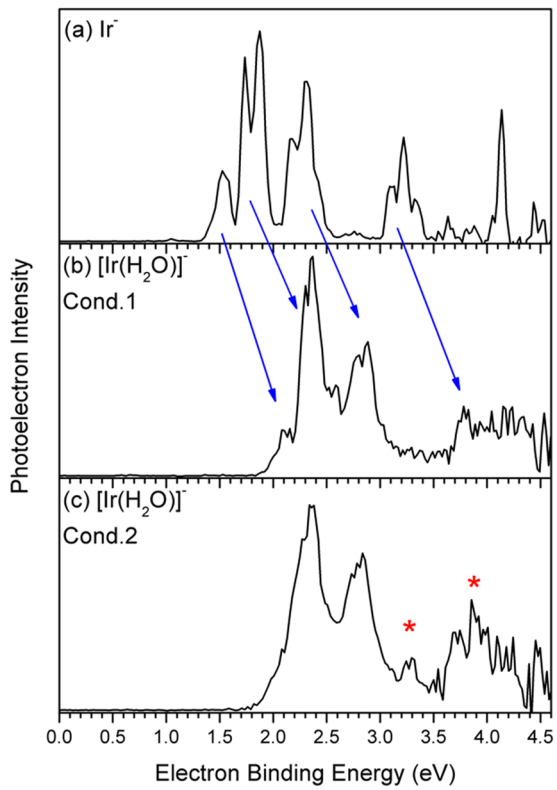

FIG. 2. Photoelectron spectra of the atomic metal anions, Ir^-, (in the top panel), and $[Ir(H_2O)]^-$ anions (in the two lower panels). All of these anion photoelectron spectra were measured using the fourth harmonic (4.66 eV/photon) of an Nd:YAG laser. Blue arrows link Ir^- peaks in (a) to their corresponding blue-shifted peaks in $Ir^-(H_2O)$ anion–molecule complexes in (b). Red stars in (c) mark new structural isomers formed under Cond. 2 source conditions.

Computational

DFT calculations were carried out to locate intermediates formed via the reaction of Ir^- anions and water molecules. The optimized isomers in different spin multiplicities for these reaction intermediates are presented in Fig. 3, along with their relative energies. We categorized all isomers into the three types previously mentioned. Structures A and B are type (i) isomers, and can be considered to be an Ir^- anion, solvated by (physisorbed with) a water molecule. The ground state of the iridium anion is a triplet, with $[Xe]4f^{14}5d^86s^2$ electronic configuration, which makes the ground state of $Ir^-(H_2O)$ a triplet as well. The singlet solvation structure, A, is 1.53 eV higher in energy than the triplet isomer B. Both, isomer A and isomer B, exhibit planar structures. In isomer B, the lengths of the O–H bonds in the water moiety are 0.96 and 0.98 Å, both close to that of an isolated H_2O molecule (0.96 Å). Thus, the water moiety in isomer B remains essentially intact, with the exception that one O–H bond is slightly elongated, due to its attraction with the Ir^- anion. In type (ii) isomers, C and D, the iridium atom is inserted into an O–H bond of water, forming an $H–Ir–OH^-$ structure. This activates the water molecule and is the first step in water splitting. Triplet isomer D is lower in energy by 0.34 eV than the singlet isomer C. Turning to type (iii) isomers, the global minimum of $[Ir(H_2O)]^-$, E, features two H atoms attached to the Ir atom, yielding a $H_2–Ir–O^-$ structure. Isomer E has an $O–Ir–H_2$ dihedral angle of 53.2°, while isomer F has a planar structure with C_{2v} symmetry. Interestingly, in type (iii) isomers, the singlet is lower in energy than the triplet by 0.22 eV, suggesting that a spin-crossover may take place when intermediates transform from type (ii) to type (iii).

To explore the presence or absence of these structures, calculated VDE values from each anionic isomer to both the doublet and quartet states of its corresponding neutral were compared with the experimental values (see Table I). Note that all calculated VDE values are lower than the photodetachment photon energy (4.66 eV) used in this work. VDE values for isomers A (0.64 eV) and C (1.67 eV) are significantly lower than the observed experimental value (2.11 ± 0.05 eV), suggesting the absence of isomers A and C in the ion beam. However, even with calculated VDE values, the complex $[Ir(H_2O)]^-$ photoelectron spectra cannot be explained fully due to photodetachment transitions to the excited electronic states of each isomer. Thus, to gain additional insight, we conducted TD-DFT excited-state calculations on all neutral forms of the isomers at their anionic geometries. The complete list of excitation energies is provided in Table S1 in the supplementary material. To further investigate how each isomer contributed to the experimental

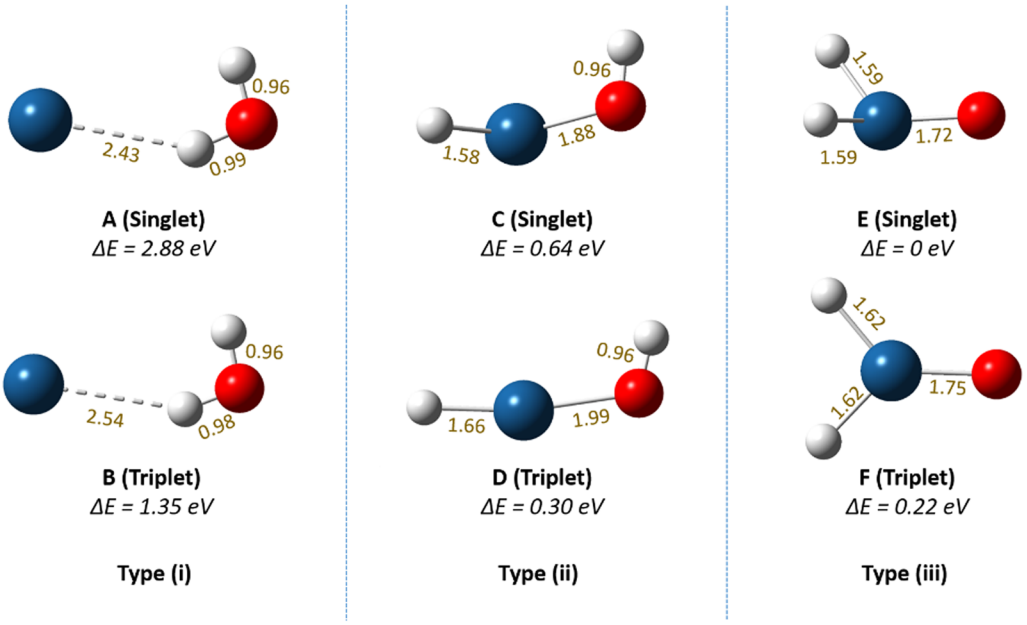

FIG. 3. Optimized structures of $[Ir(H_2O)]^-$ categorized as three types. (i) Ir^- anion is solvated by a water molecule; (ii) only one O–H bond is broken; (iii) two O–H bonds are broken. The relative energies of $[Ir(H_2O)]^-$ are listed below each structure. Bond lengths are also shown in each structure.

spectra, we plotted the simulated density of states (DOS) spectra for isomers B, D, E, and F in Fig. 4, in order to compare them with the experimental spectra. In the DOS spectra, the first stick on the left, i.e., the one at low electron binding energy, corresponds to the ground state of the neutral, while other sticks at higher EBE represent the electronically excited states of the neutral. The simulated spectrum of isomer B displays two discernible bands ranging from 2.0 to 2.5 and 2.5 to 3.0 eV, followed by three lower intensity peaks at higher EBE. In the top panel of Fig. 4, the experimental spectrum collected under condition 1 is well reflected by the simulated spectrum of isomer B. This implies that the anionic isomer in which the Ir^- anion is solvated by a water molecule dominates the photoelectron spectrum of $[Ir(H_2O)]^-$ under low ablation laser power conditions. However, at higher laser ablation power, two new spectral features appeared, i.e., at EBE = 3.25 eV and EBE = 3.85 eV [see Fig. 2(c)], strongly implying contributions from additional isomers. The highest intensity EBE features in the simulated spectra of isomers: D, F, and E occurred at 3.4, 3.0, and 4.1 eV, respectively. While not completely clear, the new features under condition 2 may well be attributed to a mixture of electronic states arising from the photodetachment of isomers: D, E, and F. In any case, the spectral profile of isomer B most closely resembles the experimental spectra, indicating that isomer B is the dominant species formed under both laser power conditions, even as condition 2 generates water activated isomers. Also, given that isomer B is 1.35 eV higher in energy than the global minimum isomer, E, yet more abundantly formed, this may imply a kinetically favorable formation pathway for isomer B.

The pathway of the $Ir^- + H_2O$ reaction through both its singlet and triplet multiplicities was explored, to better identify its reaction intermediates and to investigate the mechanism of water splitting (see Fig. 5). Reaction intermediates are labeled **IN**. Recall that $\mathbf{IN1^s}$ (isomer A) and $\mathbf{IN2^s}$ (isomer C) are not observed in the spectra due to their low VDE values. Thus, the reaction pathway being considered here starts with reactants on the triplet potential energy curve (the blue line). The reaction between the Ir^- anion and

TABLE I. Computed and experimental VDE values (in eV) for each structure in Fig. 3.

	Type (i)		Type (ii)		Type (iii)	
Isomers	A (singlet)	B (triplet)	C (singlet)	D (triplet)	E (singlet)	F (triplet)
Expt. VDE	2.11 ± 0.05		N/A		N/A	
Calc. VDE (doublet)	1.19	2.72	1.67	3.01	2.31	2.54
Calc. VDE (quartet)	0.64	2.16	2.23	2.45	3.20	2.95

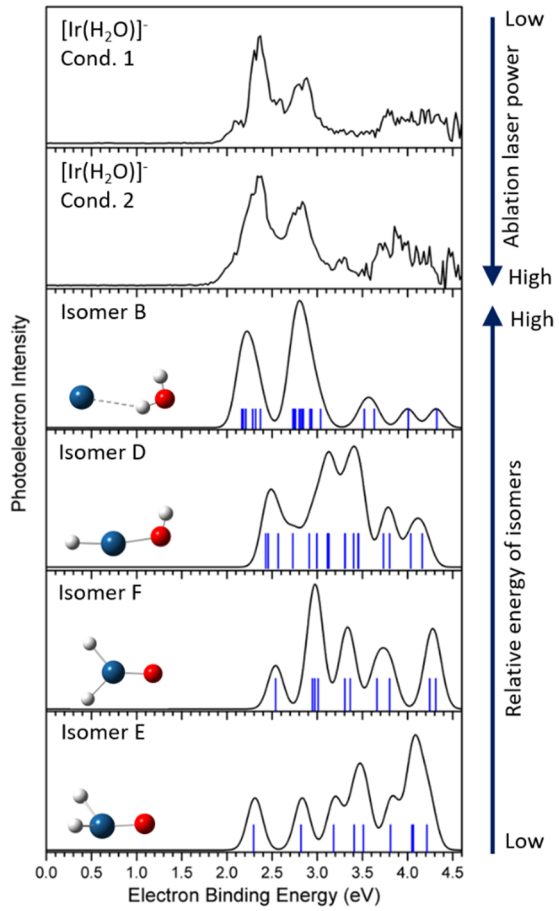

FIG. 4. Comparison between the experimental photoelectron spectra under two laser power conditions and the simulated DOS (density of states) spectra of the low-lying isomers of the $[Ir(H_2O)]^-$ clusters. The simulated spectra were obtained by fitting the distribution of the transition lines with unit-area Gaussian functions having 0.2 eV full width at half maximum (FWHM). The vertical lines (sticks) are the transitions obtained, based on the theoretically calculated VDE values and excitation energies.

a water molecule is initiated via the formation of an entrance channel ion–molecule complex, i.e., $Ir^-(H_2O)$. This barrierless process forms the triplet **IN1^t**: the physisorbed adduct with a relatively long Ir–H distance (2.54 Å). In order for **IN1^t** to insert the Ir^- anion into the O–H bond, the Ir atom needs to move beyond the H_2O plane to approach the O atom. Meanwhile, the distance of Ir–H and Ir–O is shortened to 1.59 and 2.35 Å, respectively, forming the Ir–H–O triangle in the first transition state **TS1^t**. **TS1^t** is located 1.18 eV above the **IN1^t** and 0.69 eV above the entrance channel of the entire reaction. After overcoming **TS1^t**, the rupture of the first O–H bond begins to take place, forming **IN2^t** exothermally relative to **IN1^t** by 1.05 eV. The second transition state, **TS2^t**, is characterized by another hydrogen transfer from O onto Ir and is 1.25 eV above **IN2^t**. As the H atom gets closer to Ir, breakage of the second O–H bond leads to **IN3$^{s/t}$**. This second O–H bond insertion process from **IN2^t** to **IN3^s** is also exothermic by 0.30 eV. Interestingly, **IN3^s** is lower than **IN3^t**, while all other singlet **IN**s and **TS**s are higher than triplets in energy. This energy inversion necessitates triplet–singlet spin crossing around **IN3$^{s/t}$**. We searched and found two Minimum Energy Crossing Points (**MECP**s), where a singlet and a triplet are isoenergetic. The first **MECP1**, found between **TS2** and **IN3**, has a H–H bond distance of 2.34 Å, which is shorter than **IN3^t** (2.44 Å), but longer than **IN3^s** (2.10 Å). The dihedral angle of O–Ir–H_2 in **MECP1** is 25.7°, between the angles seen in **IN3^t** (0°) and **IN3^s** (53.2°). Spin crossing can make both **TS2^t** to **IN3^t** and **TS2^t** to **IN3^s** pathways accessible. After passing through the **IN3^s**, the activation intermediates encounter the second **MECP2**, where the H–H distance is significantly shortened to 1.71 Å, showing an evident tendency toward $H_2 + IrO^-$ products. Compared to the reaction from $M^- + H_2O$ to $H_2 + MO^-$ (where M = Pt, Pd, and Ni), which is endothermic according to our previous study,[38] $H_2 + IrO^-$ lies 0.03 eV below the entrance channel, making the entire reaction slightly exothermic.

Overall, Ir^- anion reaction with a water molecule sequentially goes through **IN1^t**, **TS1^t**, **IN2^t**, **TS2^t**, and **IN3$^{s/t}$** to form H_2 and triplet IrO^-. By combining information gleaned from our photoelectron spectrum and our above reaction mechanism study, we can confirm that $[Ir(H_2O)]^-$ isomers B, D, E, and F all—exist in the ion beam. Additionally, only **TS1^t** is higher than the entrance channel in energy along the entire pathway, which impedes the transformation from **IN1^t** (isomer B) to latter intermediates. The trapped **IN1^t** explains the domination of physisorbed adduct (isomer B) in the photoelectron spectrum under the low ablation power condition [Fig. 2(b)]. When excess energy was provided into the reaction under the high ablation laser power circumstance, one sees the formation of other chemically activated complexes (isomer D, E, and F) in the photoelectron spectrum [Fig. 2(c)], as well as the final product, IrO^-, in the mass spectrum [Fig. 1(b)].

Electrons play an important role in the reduction of H_2O into H_2. Herein, we examine the net charge on every atom in critical intermediates and transition states and plot the corresponding 2D ELF contours in Fig. 6, to study the electron flow between atoms during the water splitting reaction. Ir stays negatively charged (−0.949 *e*), almost the same as a free Ir anion (−1 *e*), in **IN1^t**. The ELF contour in the lower panel of Fig. 6(a) illustrates that Ir^- and H_2O are clearly separated, revealing that the electrons are localized in these fragments. The dark color (low ELF value) means no covalent bond is formed between Ir and H1 atom, proving that electrostatic forces govern the interaction between Ir^- anion and H_2O molecule. When Ir approaches the H_2O in **TS1^t**, both Ir and H experience significant changes in charge. Due to the identical electronegativity of Ir and H (2.2), the excess negative charge on Ir flows into the H1 atom. The moderate negative charge accumulation on O (−0.986 to −1.081 *e*) from **IN1^t** to **TS1^t** is driven by the notable electronegativity difference between O (3.4) and Ir/H (2.2). From **TS1^t** to **IN2^t**, NBO analysis also shows that the net charge of the O atom is nearly unperturbed (−1.081 to −1.089 *e*), while the net charge on Ir escalates from −0.573 to +0.034 *e* along the first activation step. Thus, Ir serves as an essential electron donor when the first hydrogen transfer occurs. Unlike **IN1^t**, the ELF contours are greatly delocalized over the whole molecule in the **TS1^t** and **IN2^t** [Figs. 6(a) and 6(b)], manifesting the formation of the Ir–H1 covalent bond. In Fig. 6(c), the Ir–O bond displays a patent ionic bond feature, because of the low ELF values (dark color) in the middle of the Ir–O axis. To

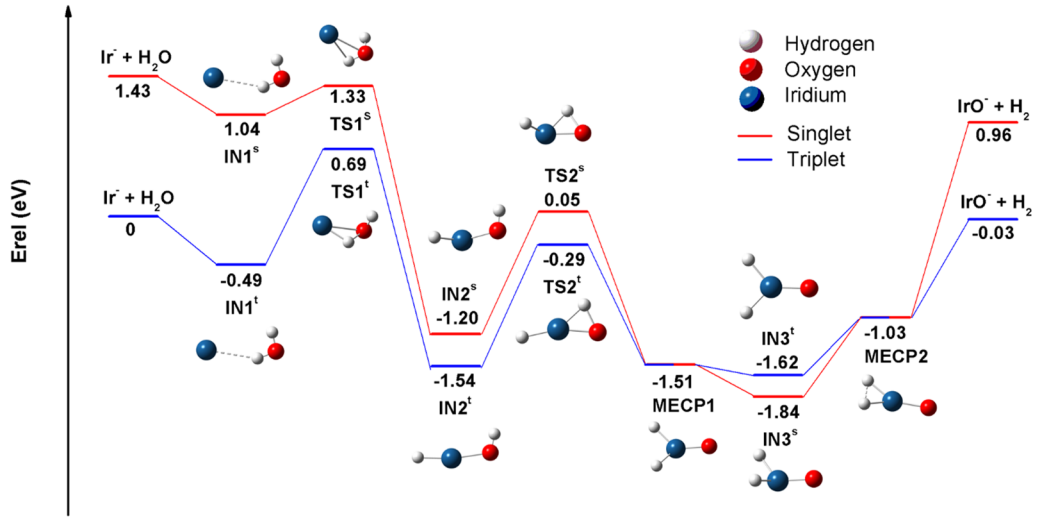

FIG. 5. Calculated reaction pathways for H_2O + Ir^- anion. Energies are given in eV. The total energy of isolated Ir^- (triplet) and H_2O is set at 0 eV. Structures labeled IN are reaction intermediates, TS are transition states. Superscripts t and s indicate triplet and singlet states, respectively. The Minimum Energy Crossing Points (MECPs), are schematically indicated with bicolor at the crossings of the two potential energy surfaces.

further trigger the breakage of the second O–H bond, O starts to be a successor of Ir to provide electrons. From **IN2^t** to **TS2^t**, 0.18 *e* of negative charge transfers from O to the H2 atom, elongating and weakening the O–H bond. Meanwhile, the green color between Ir and H2 atoms and the dark blue color between O and H2 atoms in the ELF contour [Fig. 6(d)] reveal the formation of the Ir–H2 bond and the cleavage of the O–H2 bond. After overcoming **TS2^t**, the net charge is evenly shared in both H atoms (−0.083 *e*) in **IN3^s**, close to 0 *e* in the neutral H_2 molecule. In Fig. 6(e), the 2D contour is displayed on the H1–Ir–O plane, so that the H2 atom is out of plane. Although the ELF around the H2 atom is not fully shown on this selected plane, one can still see vaguely blue electron distributions between H1 and H2, which builds the foundation for forming an H–H bond in the H_2 molecule later.

CONCLUSIONS

To summarize, we have demonstrated that a single atomic iridium anion can both activate and split a single water molecule. Both activation intermediates, $[Ir(H_2O)]^-$, and one of the reaction

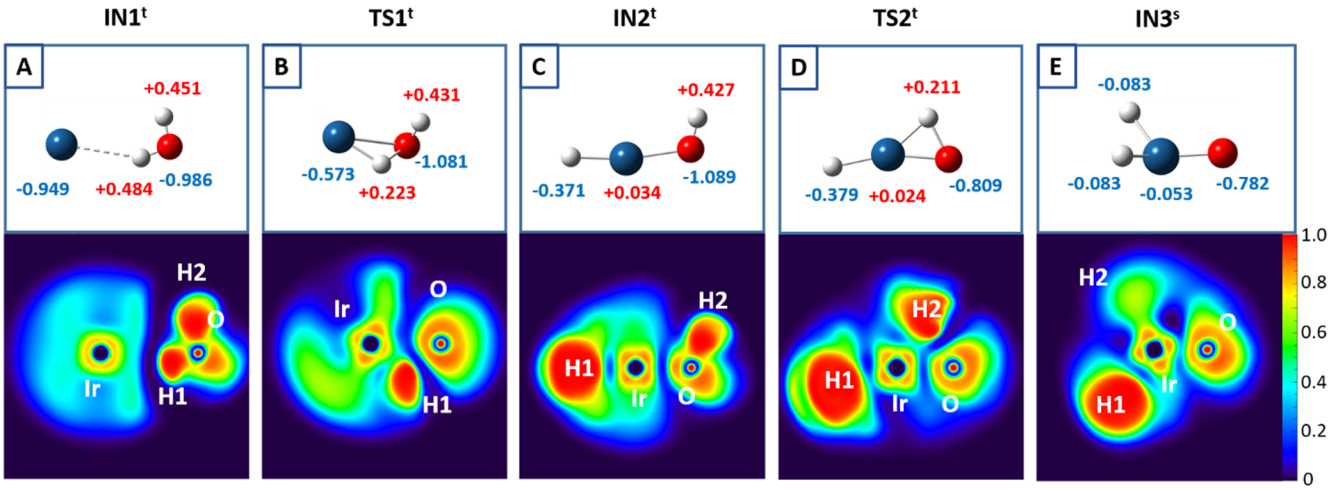

FIG. 6. NBO net charges of all atoms in lowest intermediates and transition states in energy along the reaction pathway (upper panels). Two-dimensional electron localization functions (ELF) for the species above (lower panels). IN1^t in (a), TS1^t in (b), IN2^t in (c), TS2^t in (d), and IN3^s in (e). Atoms are labeled and numbered in the ELF contour. The ELF distributions are shown on the Ir–H–O plane and are described chromatically. A large ELF value means that electrons are greatly localized.

products, IrO^-, were observed in the mass spectrum. Identification of multiple isomers for $[Ir(H_2O)]^-$ was accomplished by a combination of anion photoelectron spectroscopy and DFT calculations. Mechanistic analysis shows that the spin crossover between singlet and triplet surfaces provides access to two reaction channels. The exothermic energetics of the overall reaction was compared with the reaction of water with single Pt/Pd/Ni anions. The NBO partial charge and ELF contour analysis reveals that Ir serves as an electron donor to activate water. This work provides insight into the nature of water activation and splitting with a single Ir atom at the molecular level, shedding light on the design of new Ir SACs in the condensed phase.

SUPPLEMENTARY MATERIAL

See the supplementary material for details of additional theoretical results, including excitation energies of neutral $Ir(H_2O)$, and Cartesian coordinates of optimized structures are presented therein.

ACKNOWLEDGMENTS

This material is based on the work supported by the Air Force Office of Scientific Research (AFOSR) under Grant No. FA9550-22-1-0271 (K.H.B.).

AUTHOR DECLARATIONS

Conflict of Interest

The authors have no conflicts to disclose.

Author Contributions

Z.Z., G.L., S.M.C., and R.M.H. participated in the anion photoelectron spectroscopic measurements. Z.Z. and Y.C. performed the theoretical calculations. K.H.B. supervised the experimental work. Z.Z. and K.H.B. drafted the manuscript.

Zhaoguo Zhu: Formal analysis (equal); Writing – original draft (equal). **Gaoxiang Liu**: Formal analysis (equal); Investigation (equal). **Sandra M. Ciborowski**: Formal analysis (equal); Investigation (equal). **Yulu Cao**: Validation (equal). **Rachel M. Harris**: Writing – review & editing (supporting). **Kit H. Bowen**: Supervision (lead); Writing – review & editing (lead).

DATA AVAILABILITY

The data that support the findings of this study are available from the corresponding author upon reasonable request.

REFERENCES

[1] I. Roger, M. A. Shipman, and M. D. Symes, Nat. Rev. Chem. **1**, 0003 (2017).
[2] J. Wang, W. Cui, Q. Liu, Z. Xing, A. M. Asiri, and X. Sun, Adv. Mater. **28**, 215 (2016).
[3] B. You and Y. Sun, Acc. Chem. Res. **51**, 1571 (2018).
[4] Z. Wang, C. Li, and K. Domen, Chem. Soc. Rev. **48**, 2109 (2019).
[5] Q. Wang and K. Domen, Chem. Rev. **120**, 919 (2019).
[6] S. Ye, C. Ding, R. Chen, F. Fan, P. Fu, H. Yin, X. Wang, Z. Wang, P. Du, and C. Li, J. Am. Chem. Soc. **140**, 3250 (2018).
[7] J. Feng, H. Huang, S. Yan, W. Luo, T. Yu, Z. Li, and Z. Zou, Nano Today **30**, 100830 (2020).
[8] J. E. Funk, Int. J. Hydrogen Energy **26**, 185 (2001).
[9] A. Kudo and Y. Miseki, Chem. Soc. Rev. **38**, 253 (2009).
[10] X. Zou and Y. Zhang, Chem. Soc. Rev. **44**, 5148 (2015).
[11] C. Gao, J. Low, R. Long, T. Kong, J. Zhu, and Y. Xiong, Chem. Rev. **120**, 12175 (2020).
[12] A. Wang, J. Li, and T. Zhang, Nat. Rev. Chem. **2**, 65 (2018).
[13] F. Zhang, Y. Zhu, Q. Lin, L. Zhang, X. Zhang, and H. Wang, Energy Environ. Sci. **14**, 2954 (2021).
[14] Q. Wang, X. Huang, Z. L. Zhao, M. Wang, B. Xiang, J. Li, Z. Feng, H. Xu, and M. Gu, J. Am. Chem. Soc. **142**, 7425 (2020).
[15] W. H. Lai, L. F. Zhang, W. B. Hua, S. Indris, Z. C. Yan, Z. Hu, B. Zhang, Y. Liu, L. Wang, M. Liu, R. Liu, Y. X. Wang, J. Z. Wang, Z. Hu, H. K. Liu, S. L. Chou, and S. X. Dou, Angew. Chem. **131**, 11994 (2019).
[16] Z. Zhang, C. Feng, C. Liu, M. Zuo, L. Qin, X. Yan, Y. Xing, H. Li, R. Si, S. Zhou, and J. Zeng, Nat. Commun. **11**, 1215 (2020).
[17] K. Jiang, M. Luo, M. Peng, Y. Yu, Y.-R. Lu, T.-S. Chan, P. Liu, F. M. F. de Groot, and Y. Tan, Nat. Commun. **11**, 2701 (2020).
[18] J. Yin, J. Jin, M. Lu, B. Huang, H. Zhang, Y. Peng, P. Xi, and C.-H. Yan, J. Am. Chem. Soc. **142**, 18378–18386 (2020).
[19] Y. Zhang, C. Wu, H. Jiang, Y. Lin, H. Liu, Q. He, S. Chen, T. Duan, and L. Song, Adv. Mater. **30**, 1707522 (2018).
[20] T. He, S. Chen, B. Ni, Y. Gong, Z. Wu, L. Song, L. Gu, W. Hu, and X. Wang, Angew. Chem. **130**, 3551–3556 (2018).
[21] Z. Lei, W. Cai, Y. Rao, K. Wang, Y. Jiang, Y. Liu, X. Jin, J. Li, Z. Lv, S. Jiao, W. Zhang, P. Yan, S. Zhang, and R. Cao, Nat. Commun. **13**, 24 (2022).
[22] X. Zheng, J. Tang, A. Gallo, J. A. G. Torres, X. Yu, C. J. Athanitis, E. M. Been, P. Ericius, H. Mao, S. C. Fakra, C. Song, R. C. Davis, J. A. Reimer, J. Vinson, M. Bajdich, and Y. Cui, Proc. Natl. Acad. Sci. U. S. A. **118**, e2101817118 (2021).
[23] H. Zhang, H. Wu, Y. Jia, B. Yin, L. Geng, Z. Luo, and K. Hansen, Commun. Chem. **3**, 148 (2020).
[24] H. Zhang, M. Zhang, Y. Jia, L. Geng, B. Yin, S. Li, Z. Luo, and F. Pan, J. Phys. Chem. Lett. **12**, 1593 (2021).
[25] S. M. Lang, I. Fleischer, T. M. Bernhardt, R. N. Barnett, and U. Landman, Nano Lett. **13**, 5549 (2013).
[26] S. M. Lang, T. M. Bernhardt, D. M. Kiawi, J. M. Bakker, R. N. Barnett, and U. Landman, Angew. Chem., Int. Ed. **54**, 15113 (2015).
[27] S. M. Lang, T. M. Bernhardt, D. M. Kiawi, J. M. Bakker, R. N. Barnett, and U. Landman, Phys. Chem. Chem. Phys. **18**, 15727 (2016).
[28] M. R. Fagiani, X. Song, S. Debnath, S. Gewinner, W. Schöllkopf, K. R. Asmis, F. A. Bischoff, F. Müller, and J. Sauer, J. Phys. Chem. Lett. **8**, 1272 (2017).
[29] M. L. Weichman, S. Debnath, J. T. Kelly, S. Gewinner, W. Schöllkopf, D. M. Neumark, and K. R. Asmis, Top. Catal. **61**, 92 (2018).
[30] J. A. DeVine, A. Abou Taka, M. C. Babin, M. L. Weichman, H. P. Hratchian, and D. M. Neumark, J. Chem. Phys. **148**, 222810 (2018).
[31] C. Geng, J. Li, T. Weiske, and H. Schwarz, J. Am. Chem. Soc. **140**, 9275 (2018).
[32] Y. Chen, J. Jin, K. Xin, W. Yu, X. Xing, X. Wang, and G. Wang, Phys. Chem. Chem. Phys. **21**, 15639 (2019).
[33] X. Jian, K. Xin, J. Hu, L. Zhang, X. Wang, and G. Wang, J. Phys. Chem. A **125**, 5054 (2021).
[34] K. Xin, Y. Chen, L. Zhang, B. Xu, X. Wang, and G. Wang, Phys. Chem. Chem. Phys. **23**, 528 (2021).
[35] M. Wang, C.-X. Sun, Y. Zhao, J.-T. Cui, and J.-B. Ma, J. Phys. Chem. A **123**, 7576 (2019).
[36] A. J. McMahon and C. C. Jarrold, Phys. Chem. Chem. Phys. **22**, 27936 (2020).
[37] G. L. Hou, T. Yang, M. Li, J. Vanbuel, O. V. Lushchikova, P. Ferrari, J. M. Bakker, and E. Janssens, Angew. Chem., Int. Ed. **60**, 27095 (2021).
[38] G. Liu, E. Miliordos, S. M. Ciborowski, M. Tschurl, U. Boesl, U. Heiz, X. Zhang, S. S. Xantheas, and K. Bowen, J. Chem. Phys. **149**, 221101 (2018).
[39] M. W. Schmidt and M. S. Gordon, Z. Phys. Chem. **227**, 1301 (2013).
[40] C. Bussai, S. Krüger, G. N. Vayssilov, and N. Rösch, Phys. Chem. Chem. Phys. **7**, 2656 (2005).
[41] S. Krüger, C. Bussai, A. Genest, and N. Rösch, Phys. Chem. Chem. Phys. **8**, 3391 (2006).
[42] K. Balasubramanian and D. Dai, J. Chem. Phys. **93**, 7243 (1990).

[43]S. Castillo, V. Bertin, E. Solano-Reyes, H. Luna-García, A. Cruz, and E. Poulain, Int. J. Quantum Chem. **70**, 1029 (1998).
[44]M. Okumura, Y. Irie, Y. Kitagawa, T. Fujitani, Y. Maeda, T. Kasai, and K. Yamaguchi, Catal. Today **111**, 311 (2006).
[45]S. M. Ciborowski, R. Buszek, G. Liu, M. Blankenhorn, Z. Zhu, M. A. Marshall, R. M. Harris, T. Chiba, E. L. Collins, S. Marquez, J. A. Boatz, S. D. Chambreau, G. L. Vaghjiani, and K. H. Bowen, J. Phys. Chem. A **125**, 5922 (2021).
[46]F.-X. Li, X.-G. Zhang, and P. B. Armentrout, Int. J. Mass Spectrom. **255-256**, 279 (2006).
[47]A. Halder, C. Liu, Z. Liu, J. D. Emery, M. J. Pellin, L. A. Curtiss, P. Zapol, S. Vajda, and A. B. F. Martinson, J. Phys. Chem. C **122**, 9965 (2018).
[48]F.-X. Li, X.-G. Zhang, and P. B. Armentrout, J. Phys. Chem. B **109**, 8350 (2005).
[49]W. Li, X. Wu, Z. Liu, H. Wu, D. Zhang, and X. Ding, J. Phys. Chem. Lett. **11**, 8346 (2020).
[50]O. W. Wheeler, M. Salem, A. Gao, J. M. Bakker, and P. B. Armentrout, Int. J. Mass Spectrom. **435**, 78 (2019).
[51]P. B. Armentrout, Chem. - Eur. J. **23**, 10 (2017).
[52]P. Cheng, G. K. Koyanagi, and D. K. Bohme, J. Phys. Chem. A **111**, 8561 (2007).
[53]M. Gerhards, O. C. Thomas, J. M. Nilles, W.-J. Zheng, and K. H. Bowen, J. Chem. Phys. **116**, 10247 (2002).
[54]J. Ho, K. M. Ervin, and W. C. Lineberger, J. Chem. Phys. **93**, 6987 (1990).
[55]J.-D. Chai and M. Head-Gordon, J. Chem. Phys. **128**, 084106 (2008).
[56]J.-D. Chai and M. Head-Gordon, Phys. Chem. Chem. Phys. **10**, 6615 (2008).
[57]T. H. Dunning, Jr., J. Chem. Phys. **90**, 1007 (1989).
[58]R. A. Kendall, T. H. Dunning, Jr., and R. J. Harrison, J. Chem. Phys. **96**, 6796 (1992).
[59]D. Figgen, K. A. Peterson, M. Dolg, and H. Stoll, J. Chem. Phys. **130**, 164108 (2009).
[60]M. J. Frisch, G. W. Trucks, H. B. Schlegel, G. E. Scuseria, M. A. Robb, J. R. Cheeseman, G. Scalmani, V. Barone, B. Mennucci, G. A. Petersson, H. Nakatsuji, M. Caricato, X. Li, H. P. Hratchian, A. F. Izmaylov, J. Bloino, G. Zheng, J. L. Sonnenberg, M. Hada, M. Ehara, K. Toyota, R. Fukuda, J. Hasegawa, M. Ishida, T. Nakajima, Y. Honda, O. Kitao, H. Nakai, T. Vreven, J. A. Montgomery, Jr., J. E. Peralta, F. Ogliaro, M. Bearpark, J. J. Heyd, E. Brothers, K. N. Kudin, V. N. Staroverov, R. Kobayashi, J. Normand, K. Raghavachari, A. Rendell, J. C. Burant, S. S. Iyengar, J. Tomasi, M. Cossi, N. Rega, J. M. Millam, M. Klene, J. E. Knox, J. B. Cross, V. Bakken, C. Adamo, J. Jaramillo, R. Gomperts, R. E. Stratmann, O. Yazyev, A. J. Austin, R. Cammi, C. Pomelli, J. W. Ochterski, R. L. Martin, K. Morokuma, V. G. Zakrzewski, G. A. Voth, P. Salvador, J. J. Dannenberg, S. Dapprich, A. D. Daniels, O. Farkas, J. B. Foresman, J. V. Ortiz, J. Cioslowski, and D. J. Fox, Gaussian 09, Revision D.01, Gaussian, Inc., Wallingford, CT, 2013.
[61]E. D. Glendening, A. E. Reed, J. E. Carpenter, and F. Weinhold, NBO Version 3.1, 1998.
[62]H. Wang, Y. Jae Ko, X. Zhang, G. Gantefoer, H. Schnoeckel, B. W. Eichhorn, P. Jena, B. Kiran, A. K. Kandalam, and K. H. Bowen, J. Chem. Phys. **140**, 124309 (2014).
[63]G. Liu, Z. Zhu, M. Marshall, M. Blankenhorn, and K. H. Bowen, J. Phys. Chem. A **125**, 1747 (2021).
[64]J. N. Harvey, M. Aschi, H. Schwarz, and W. Koch, Theor. Chem. Acc. **99**, 95 (1998).
[65]T. Lu and F. Chen, J. Comput. Chem. **33**, 580 (2012).
[66]A. Savin, R. Nesper, S. Wengert, and T. F. Fässler, Angew. Chem., Int. Ed. **36**, 1808 (1997).